Lasers in Manufacturing Conference 2021

Ultra-short pulse laser micro-machining by spatially shaped ps- and fs-pulses for depth-selective µ-TLM resistivity test structures in TCO contact layers

Stephan Krause[a,b,*], Stefan Lange[b], Gao Yiding[b], Volker Naumann[b], Christian Hagendorf[b], Paul T. Miclea[a,b]

[a]*Centre for Innovation Competence SiLi-nano, Martin-Luther-University Halle-Wittenberg, Karl-Freiherr-von-Fritsch-Straße 3, 06120 Halle (Saale), Germany*
[b]*Fraunhofer Center for Silicon Photovoltaics CSP, Otto-Eissfeldt-Str. 12, 06120 Halle (Saale), Germany*

Abstract

Precise measurements of the electrical sheet and contact resistivity of individual layers, isolating trenches and homogenous ablation areas are required in many applications ranging from photovoltaics, opto-electronic devices to sensor technologies. We applied spatially shaped ultra-short pulse laser micro-machining for a high precision micro-machining approach for µ-TLM test structures. µ-TLM structures are fabricated with enhanced layer selectivity by matching of pulse overlapping based on rectangular spots in µm-dimensions.

Ultrashort pulses by 10 ps and 200 fs (515/532/1030 nm) as well as optical beam shaping elements for redistribution to top-hat intensity profiles enables a selective removal of the top TCO. Thus, thermal damage is minimized in the underlying material and multilayer adjacent region of the laser trenches by ultrafast ablation mechanism. Morphology and microstructure of heat-affected zones were characterized by high-resolution transmission electron microscopy to optimize laser recipes for enhancing ablation selectivity. Finally, the optimized structures were tested in resistivity measurements of various multilayer systems with highly resistive interface layers.

Keywords: ultra-sort pulses; micro-machining; µ-TLM; top-Hat profile; transparent conductive layers

1. Introduction

Laser ablation processes are used for layer-selective micro-structuring of various thin film systems on rigid or flexible substrates ranging from display technology, LED devices to organic and inorganic photovoltaics (PV)

* Corresponding author. Tel.: : +49-345-55895412
E-mail address: stephan.krause@physik.uni-halle.de .

thin films. The use of ultra-short laser pulses with less than a few tens of pico-second pulse durations allows an enhanced ablation selectivity of single layers due to non-thermal material interaction processes.

Next generation PV concepts like silicon heterojunction technology (HJT), tunnel-oxide passivated contacts (TOPCon), or perovskite solar cells consisting of thin film multilayer stacks are able to minimize the electrical losses in the semiconductor stack more efficiently. This requires the use of several transparent conductive oxide (TCO) layers, the contacts at the front and the rear as well as electrical interconnection of the two sub-cells that play a central role for charge transport and for increasing the electro-optical performance. The properties of the transparent, selective contact layers have to be optimized for reduced series resistivity losses and durability under processing conditions. Measuring sheet resistance of TCO sublayers and interfacial electrical as well as material properties is a challenge to established industrial measuring standards. To optimize the relevant manufacturing processes, contact resistance measurement techniques are required that are likewise inexpensive, versatile in application and easy to use.

In this work we applied an optimized process for µ-TLM test structures processing [Kaufmann2015] for resistivity measurements based on ps- and fs-laser micro machining [Krause2016]. The use of ultra-short laser pulses should enhance the vertical ablation selectivity to a removal of the metal/TCO with less modification of the remaining material. In addition, a minimization of the lateral dimensions due to more precise laser structuring for the µ-TLM test structures can lead to improvement of the maximal measurable contact resistivity. Thus, changes of the micro-electrical interface properties induced by experimental deposition parameters or post-deposition treatments can be assessed with higher resolution.

The method is applied to metal/TCO/glass stacks as model system, in which the metal-semiconductor junction carries ultra-low contact resistivities. Besides electrical sheet and contact resistivity values of the individual layers and interfaces, respectively, ablation thresholds and depth profiles were determined to propose laser receipts for selective area removal, vertically in nm- as well as lateral from μm^2- to mm^2-dimensions. For an improvement of the removal homogeneity and minimization of the film modification due to laser impact we used beam shapers for a redistribution of the gaussian laser intensity profiles to rectangular top-hat profiles. Therefore, smoother intensity profiles for fs- and ps-pulses slightly above the ablation threshold tried to improve the pulse-to-pulse matching which is necessary for the µ-TLM test structure fabrication.

2. Experimental

2.1. Samples and instrumentation

Preliminary beam shaping and alignment adjustments were performed on a SiN_x/Si layer stack consisting of a 70 nm SiN_x layer deposited by PECVD on a polished Si wafer. Subsequently, multilayer stacks of Al/ZnO:Al/glass were used as model system for our µ-TLM laser patterning investigations. Al and ZnO:Al (AZO) single layers and multilayer stacks were deposited on 10 x 10 cm^2 glass substrates by magnetron sputter deposition in pulsed DC and continuous DC mode from ceramic and metallic 8-inch targets at 300 W and 1000 W discharge power, respectively. The O_2/Ar partial pressure ratios were varied to be 1:50, 1:25 and 1:16.7 during the ZnO:Al deposition processes to change the electro-optical properties of the TCO layers. The total process pressure was kept constant at 1 Pa.

As shown in Fig. 1, sample names ZnO2, ZnO4, ZnO6 refer to different pressure ratios of 2%, 4% and 6% with $p\_O_2 \neq 0$. The sputter time was chosen to be 30 min for all AZO deposition processes, which resulted in layer

thicknesses between 750 and 900 nm. The Al layer thickness is about 100 nm. All thin film depositions took place at room temperature without intentional substrate heating.
µ-TLM test structures with pad dimensions of approximately 70 x 16 µm², 485 x 16 µm² and 1000 x 16 µm² were fabricated by means of ultrashort pulse laser micro machining for selective Al removal. The different pattern geometries allow the investigation of geometrical parameters and laser modification, in particular the influence of the laser ablation flank by changing the fraction of edge area to contact area. Micro-electrical measurements were performed in a 4-wire setup with tungsten microprobes (10 µm tip diameter) mounted to 3-axis translational stages under an optical microscope. Fig.1 at the right shows an illustration of the test structure as well as an inset of the positioned micromanipulator system under an optical microscope.

The preparation of the laser trenches was done by two different laser systems. First, the ultra-short pulses at λ = 1030 nm were generated from a femtosecond Yb:KGW laser system (Pharos from Light Conversion Ltd.), which provides pulses of 200 fs duration at a maximum repetition rate of f_{max} = 600 kHz and maximum average power of 6 W. Second, for the picosecond pulses we used the second harmonic at λ = 532 nm from a neoMos-Pico Nd:YAG laser system (NeoLase GmbH), which provides pulses of 10 ps duration at a maximum repetition rate of f_{max} = 10 MHz and maximum average power of 5 W at this wavelength.

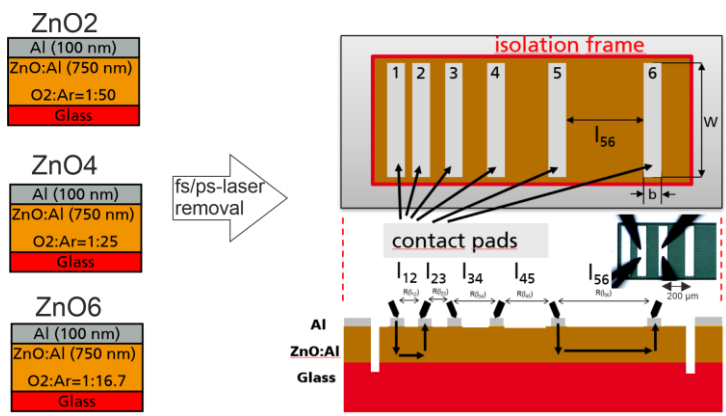

Fig. 1. Left: Schematic cross-section of the thin film model systems; three samples consist of same layer stack but slightly different deposition conditions with regard to the O_2 partial pressure were used. Right: Illustration and microscopic inset of µ-TLM test pattern after laser removal of the top metal layer. The lower cross-section shows the micro-electrical setup for the resistivity measurements.

2.2. Ultra short laser beam shaping for µ-TLM structure design

Each laser beam of both setups (fs, ps) propagates with a TEM_{00} profiles having a $M^2 < 1.4$. For the fs-pulses, we added a variable beam expander on the optical axis for controlling the input gaussian diameter in front of the top-hat beam shaper. Regarding the ps-laser system, a diffractive optical element (DoE) for 532 nm rectangular profile shaping was implemented in the optical path before the ps-laser pulses pass the focussing optic.
The top-hat focus beam shaper (FBS) is based on a diffractive beam shaping Fourier method concept (from TOPAG Lasertechnik GmbH) realized by smooth phase-modulating height profiles inside the optical element. By introducing these beam shapers into the optical paths, the diffraction limited Gaussian spot in the focal

plane is transformed into a square top-hat beam profile of both ultra-short laser sources. For the selective ablation experiments, the 200 fs pulses and 10 ps pulses were focused with f-theta lenses having a focal length of about 55 mm and 255 mm, respectively, in connection with a xy-scanner for positioning and motion control. Because of the dependence of the top hat size on the wavelength and numerical aperture of the focused beam, different top hat sizes were achieved. After laser processing, the single ablation spots and line-structuring for area removals were characterized using optical microscopy (images acquired with a Leica DM RXE-650H microscope), scanning electron microscopy (SEM) coupled with energy dispersive X-ray spectroscopy (EDX) (acquired with a JSM-7401F (JEOL) electron microscope) and profilometry (cross-sectional profiles were taken with a Bruker DektakXT stylus profilometer).
The µ-TLM test structures should consist of trenches down to the glass substrate working as isolating frames and homogenous ablation areas in µm dimensions prepared using beam shaped fs- and ps-laser processes (scheme in Fig. 1b). Laser ablated spots and trench areas were investigated by optical and scanning electron microscopy as well as profilometry which allows optical and topographical inspections. For a layer-selective thin film removal it is helpful to determine the single shot ablation thresholds and ablation characteristics of the single layer in the stack. In addition, for achieving a clean area removal using laser line structuring the influence of the pulse overlap in combination to the pulse energy and ablation depth have to be considered. By varying the scribing speed, single ablation spots as well as lines consisting of successive pulses with well-defined overlap were produced. An attenuator consisting of a half-wave plate and a thin-film polarizer was used to enable to vary the pulse energies in a precise and reproducible way. The actual pulse energies were then determined by measuring the average power in front of the samples with a thermopile detector, considering the chosen repetition frequency.

3. Results and Discussions

3.1. Gaussian-to-top-hat beam shaping adjustment based on SiN/Si reference system ablation

After the implementation of the beam shaping elements into the optical paths, we started to align the relative positioning and the adaption of the input beams for a high-quality transformation to square top-hat beam profiles of both ultra-short laser pulses. Therefore, the input beam profiles were checked via beam profilers regarding beam diameter (f.e. FBS for fs-beam shaping has a tolerance of ± 5%) and beam quality $M^2 < 1.4$ (single mode Gaussian beam TEM_{00}).
Since the optical axis were adjusted, the input beam diameter was matched to the required experimental conditions of the ps- and fs-beam shaping optical elements. Ablation experiments were performed along the z-axis of the focal plane on different z-positions. The aim was to determine the z-dependence of the pulse shape in the Rayleigh zone. That gave hints to the sensitivity of the focus position with respect to sample surface on the focal plane.

Exemplarily, Fig. 2 shows fs-ablation results at different z-positions in the focal plane a) and on a reference SiN_x/Si sample b) before and after installation of a beam shaper. SiN_x/Si was used because it is a well-known sample system in photovoltaic for UKP ablation (e.g. laser contact opening process for PERC-cell application) [Heinrich2011]. The well-defined and low SiN_x-ablation threshold were used to detect changes in the intensity profile on the ablation result due to pulse shaping and focus variation.
On the left side in Fig.2 b, the Gaussian ablation spot was generated by fs-irradiation slightly above the SiN_x ablation threshold, while in the right microscopic image of Fig.2 b the ablation geometry of the SiN_x layer after beam shaping is shown. A top hat profile at the applied focal length (the f-theta optics of f=55 mm) of about 20 µm x 23 µm was obtained and served as baseline for the experimental transfer on the Al/ZnO:Al system.

For the adjustment of the ps-laser setup we use an identical procedure to initialize the experimental requirements for the installation of the beam shaper.

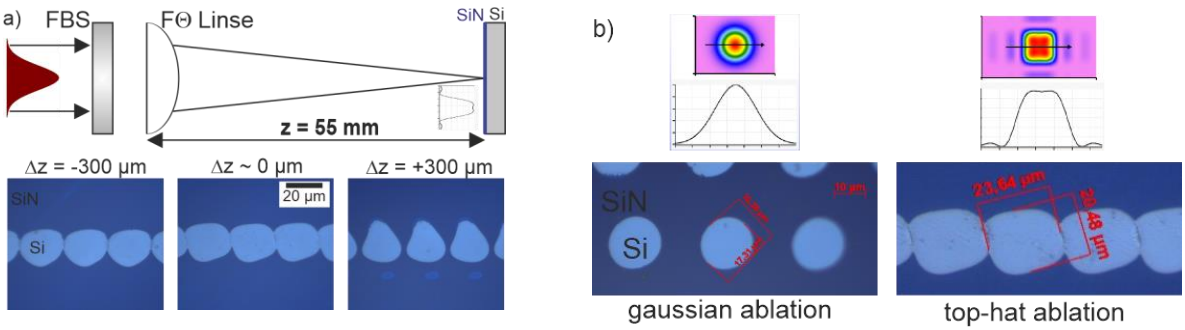

Fig. 2. a) Ablation spots in z-dependence of the focal position. The intensity profiles changes in few hundreds µm of z-dependence and diffraction order of the beam shaping. On the right b) the ablation spots without (gaussian) and with beam shaper (top-hat) on the focal position.

3.2. Determination of top-hat shaped single shot ablation threshold of the top Al-layer

For fabrication of µ-TLM patterns the laser pulses have to remove the Al-layer down to the ZnO:Al interface. Hence, a single scan process is considered where the laser pulse parameters, especially overlap and fluence, are adjusted to achieve homogenous trenches with an ablation depth according to Al layer thickness. In general, for achieving homogenous trenches inside the Al/ZnO:Al multilayer the laser fluence has to be adjusted in the range of the ablation threshold fluence of top layer. Therefore, the ablation threshold fluence of the Al top layer has been determined separately for different fluences of the applied ps- and fs-pulses.
Fig. 3 shows a plot of the ablated area of the top Al layer versus the center fluence of the almost rectangular top-hat fs- and ps-pulses for determination of the single layer ablation threshold. In general, the ablation thresholds can be derived by extrapolating to zero ablation area [Liu1982] as can be easily seen for the fs-pulses of about ~0.05 J/cm^2. Higher fluences larger than 0.2 J/cm^2 lead to larger ablated area as well as deeper rectangular spots inside the underlying ZnO:Al film.
Regarding the ps pulse regime, an ablation threshold fluence of ~0.5 J/cm^2 was observed as shown in Fig.3 bottom right. Below 0.5 J/cm^2, the laser structuring results show only optical modifications of the Al layer as visible browning at the edge profiles (Fig.3, right) but no partial removal were detected. Ps single shot ablation in the range of 0.56 J/cm^2 show several parts of modification inside the spots. The spots range from outer optical modification over a bulged rim to an inner ablated spot within the ZnO:Al layer. These laser fluences for fs- and ps-ablation thresholds of the Al top-layer are in the same range to those reported for fs- and ps-gaussian pulses [Olbrich2016].
Both ablation processes, fs pulses (1030 nm) and ps pulses (532 nm), provide a fluence window to completely and selectively remove the Al top layer from the underlying TCO (ZnO:Al) layer. The differences in the threshold fluences and crater morphologies are due to the wavelength and pulse duration difference as well as the top-hat shape.

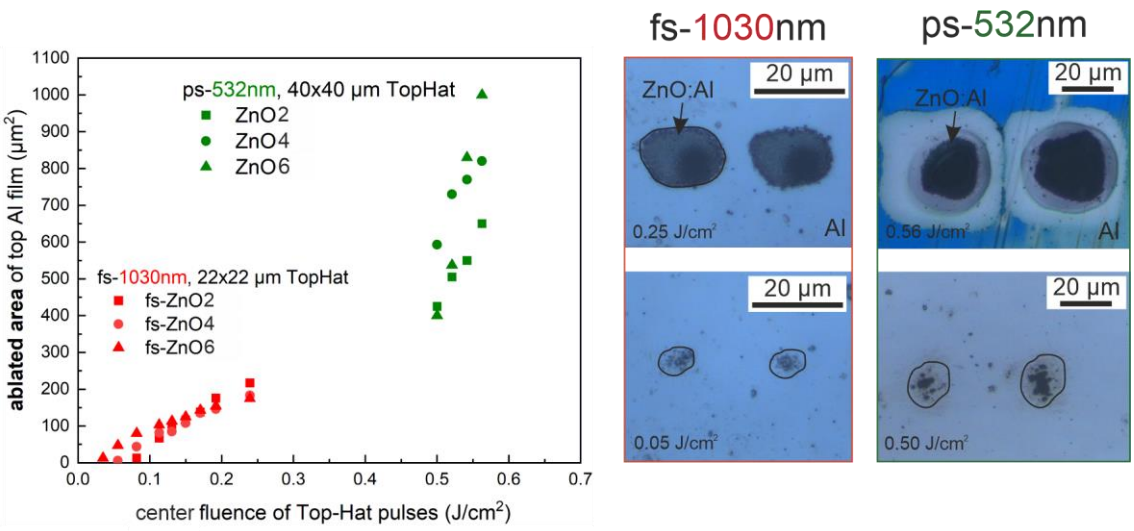

Fig. 3. Left: Ablation areas versus top hat fluences of the ultrashort pulses of the irradiated multilayer stack. Right: Light microscopy of the fs pulse and ps pulse ablation spots.

3.3. Multi-pulse top-hat patterning for selective area removal of the top layer for µ-TLM test structures

The determined single shot ablation thresholds of the fs- and ps-pulses were used to adjust the area removal for the µ-TLM pattern as homogenous as possible. Therefore, a parameter study regarding fluences slightly above the ablation threshold as well as pulse overlap variations were performed to identify the parameters for a selective large area Al ablation process with minimum damage of the underlying TCO (ZnO:Al) layer. Figure 4 shows a light microscopy overview for a fs-laser process parameter set as an example. It includes three fluence values (0.1 J/cm^2, 0.15 J/cm^2 and 0.2 J/cm^2) three different spot-to-spot distance values (10 µm, 15 µm, 20 µm) on a square field of about 250 x 250 µm^2.

On the right of Fig.3, the corresponding profilometry line scans for each constant fs-laser fluence are presented. As expected, higher pulse overlap and lower spot-to-spot distance leads to an increased ablation depth. For 0.1 J/cm^2 and 10 µm spot-to-spot distance we find a smooth area removal with an ablation depth of about 145 ± 10 nm. This indicates a complete removal of the Al layer (100 nm) and low partial ablation of the underlying TCO (ZnO:Al) layer. With respect to higher fluences, we observed a larger ablation depth down to 200 nm as well as higher roughness inside the laser-structured areas if the spot-to-spot distances increases to 20 µm for fs pulses. The deep grooves profiles of about 1 µm depth at the edges of the square fields were treated by a higher scan number to ablate down to the glass substrate and work as isolation frame.

Regarding the ps-pulse regime, we studied the multi-pulse patterning behavior for an opening of the TCO layer in the same way resulting in a laser receipt appropriate for single ablation threshold ps-fluences of 0.5 J/cm^2 and the same spot-to-spot distance of 10 µm.

For the µ-TLM structuring, multi-pulse irradiation was used, so that accumulation effects on the morphology of the opened surface could also be observed there. Since the top-hat profiles were not the same due to the different laser setups, the pulse spacing of 10 µm used cannot be directly compared. For the ps-pulses, there is a pulse overlap of approx. 75%, while for the fs pulses there is a pulse overlap of approx. 50%. The difference

of the used laser wavelength lead to differences in the ablation thresholds, but for both laser setups a process window of a complete removal of the top layer with less damage to the TCO layer could be found.

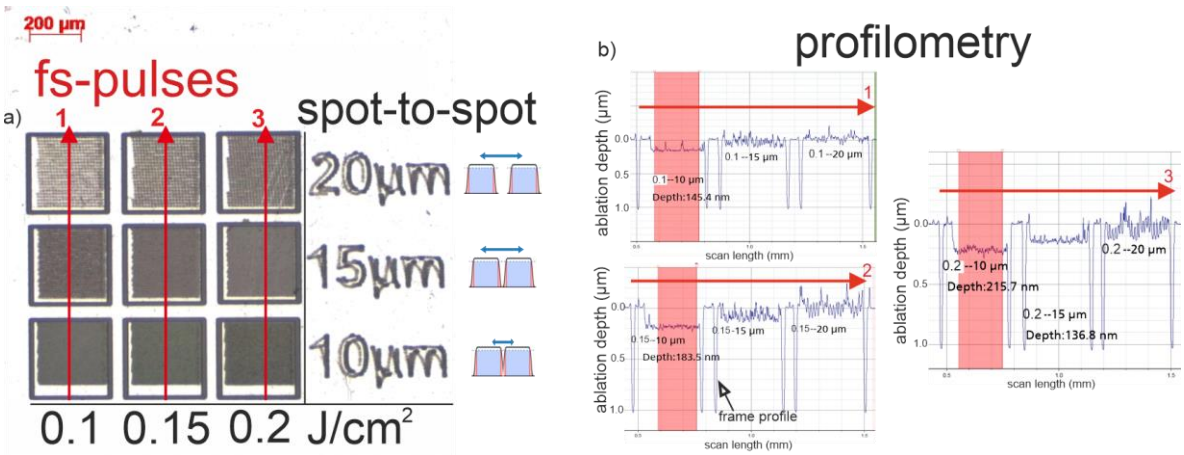

Fig. 4. a) Fs-ablation parameter study of fluence vs. spot-to-spot distance for multi-pulse top-hat patterning receipt (left). The red arrows indicate the stylus motion of the profilometry measurements illustrated on the right graphs: b) depth profiles of three fluences (f.e. 0.1 J/cm^2 refers to profile 1) in dependence of the spot-to-spot distance for pulse overlap optimization.

3.4. Micro-electrical investigation on the opened TCO and µ-TLM measurement

By using the optimized top-hat laser receipts for this stack regarding ablation thresholds for the fs- and ps-pulses and spot-to-spot overlap so far, reproducible µ-TLM test structures with homogenous ablation depth to remove the Al layer down to the TCO interface were acquired (Fig. 5). In addition, on each model sample stack a 1×1 mm^2 top Al layer ablated window was fabricated with the ps- and fs- pulses by the characterized laser receipts in the sections before and compared to reference single layer measurement of the TCO (not shown).

For the sheet resistance of the window $R_{sh-window-line}$, the 4-point probes are arranged in a line with a probe spacing of about 100 µm, which can be approximated as finite compared to the thickness of ZnO:Al. The sheet resistances of the reference single layer $R_{sh-single\ layer}$ deposited at different oxygen partial pressures were 28.85 Ω, 67.46 Ω, and 170.38 Ω. The sheet resistances of the window $R_{sh-window}$, whether the probes were arranged colinear or in square, match well with 37 Ω, 64 Ω and 200 Ω, respectively. It is important to note that the $R_{sh-window}$ does not give any hint regarding the effect of the laser on the buried ZnO:Al layer, it only provides a reference to determine the effect of the test structure on the µ-TLM extraction of R_{sh}.

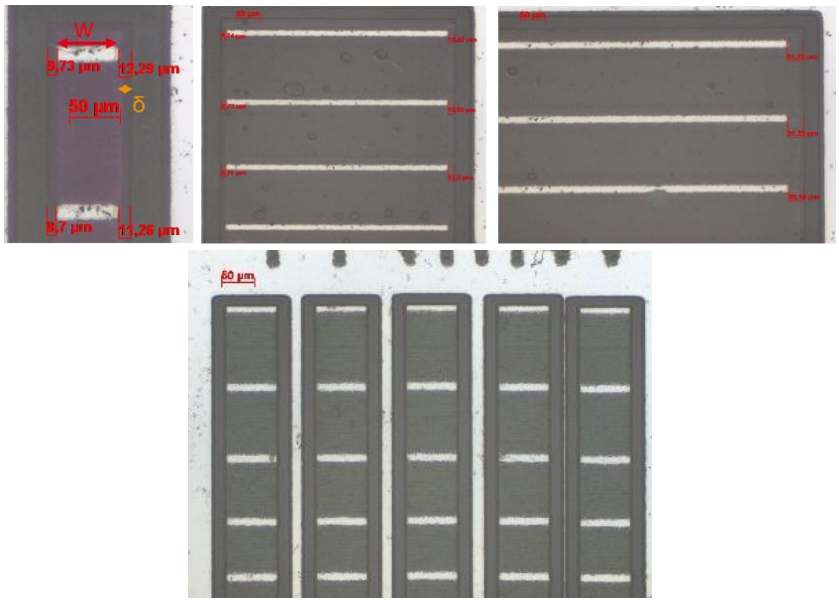

Fig 5. µ-TLM test structure after ultra-short laser processing. Edge gap measured in ps-laser pattern (above), negligible gap in fs-laser pattern (below).

A gap between the metal contact and the ZnO:Al surface is noticed in the ps-laser pattern of Fig. 5 (above) with a width δ from 10 µm to 30 µm. Since this gap is comparable to the contact length, it enables the current density to spread laterally outside the contacts such that the current flow is not strictly parallel anymore in the vicinity of the contacts. In the simplest approximation, only the influence on the sheet resistance is regarded and the 1D TLM model is modified as [Schroder2015]

$$R_T(s) = \frac{R_{sh}}{w+\delta} \cdot s + 2R_c \tag{1}$$

if the metal resistivity is not neglectable, equation (1) is further modified to (2):

$$R_T = \frac{R_{sh}}{w} \cdot s + 2R_c + R_{sh}^m \frac{w}{6 \cdot l} \tag{2}$$

For µ-TLM measurements, when the contact pad width is greater than its length, $w \gg l$, the 1D TLM model can be applied and the contact resistance R_c is given as [Schroder2015]:

$$R_c = \frac{1}{w}\sqrt{\rho_c \cdot R_{sh}}\coth\left(l\sqrt{\frac{R_{sh}}{\rho_c}}\right) \tag{3}$$

The total resistance between adjacent pads then follows from Eq. 1-3. We restrict our discussion to sheet resistances, since those are more indicative of possible changes happening to the layers, because the actual contact area is nearly untouched by the laser processes.

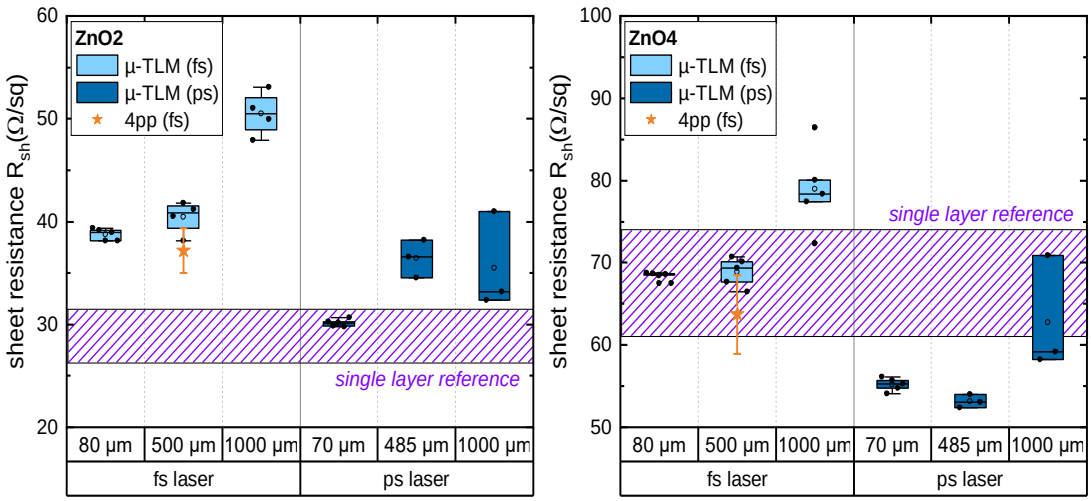

Fig. 6. 4PP-measurement in line and square shape arrangement and in line, to compare the sheet resistance.

Sheet resistances as obtained from µ-TLM, 4PP in laser-opened windows and 4PP of single layers are shown in Fig. 6 for ZnO2 and ZnO4 and different µ-TLM contact widths. The errors of 4PP values were calculated as triple standard deviation from the mean values. It can be said that sheet resistances from 4PP in ablated regions in both geometries and from µ-TLM agree well with the reference values, irrespective of temporal pulse lengths. Note the scattering in the µ-TLM data, which increases steadily with increasing contact widths, which can be ascribed to averaging the sheet resistance over a wider area.
Although both laser processes yield similar results when sheet resistances of buried layers are compared against each other and to single layer reference values, it is expected that the fs laser process enables to make much more precise statements about the specific contact resistances extracted from µ-TLM, since the edge δ between contact region and mesa insulation frame is almost negligible there and as such, parasitic current flow is minimized.

4. Conclusion

In this paper we applied an advanced approach for resistivity and thickness measurements of a model Al/ZnO:Al/glass stack, based on ps- and fs-laser micro machining of µ-TLM test structures. After thin-film deposition of the model samples, beam shapers were experimentally implemented for the laser structuring processes which shaped the Gaussian profile of the ultrashort pulses into almost square flat top-hat profiles for vertical and lateral ablation selectivity enhancement.
Ablation experiments on SiN_x/Si reference systems were used to fine-tune the adjustment of the optical setup and to characterize the process window for top-hat ablation spots.
The single-shot experiments on the Al/ZnO:Al/glass model system were investigated with profilometric and optical microscopy measurements. Modification and ablation thresholds were determined for a complete removal of the Al layer from the underlying TCO and the observed differences of the single pulse ablation

results on the Al/ZnO:Al sample system can be attributed to pulse duration dependence in the ablation behavior of thin metallic films. These determined fluences in the range of 0.1-0.5 J/cm^2 and the pulse-to-pulse distances were varied in such a way that via multipulse irradiation a homogeneous removal of the top metal layer with less damage to the conductive oxide layer underneath occurred. The area removal was evaluated regarding ablation depth and homogeneity by profilometer measurements and microstructurally clarified by SEM investigations (not shown here).

The adjusted laser recipes were used for patterning of µ-TLM test structures and sheet resistances from micro-electrical measurements of those patterns were compared with sheet resistance measurements of laser-untreated ZnO:Al layers. A good agreement between electrical properties of single layer reference samples and buried layers were found for both laser processes. The contact resistivities from fs-patterned µ-TLM structures are expected to be more precise due to minimization current spreading effects caused by insufficient mesa isolation framing. The ablation selectivity in vertical and lateral dimensions was improved due to the use of ultra-short pulses through more precise laser structuring for the µ-TLM test structures. So far, the processing work flow lead to an improvement of the maximum measurable contact resistance to the range of 0.001 mΩcm² for the micro-electrical assessment of metal/semi-conducting thin-film systems.

Acknowledgements

This work was supported by the State of Saxony Anhalt under grant number 1904/00038 (“Neue Halbleiter-Materialien 3”) and IB/LSA-project “High-precision fs-laser structuring of multilayer systems”.

References

Heinrich G., Bähr M., Stolberg K., Wütherich T., Leonhardt M., Lawerenz A., 2011, “Investigation of ablation mechanisms for selective laser ablation of silicon nitride layers”, Energy Procedia, Volume 8, p. 592-597,

Kaufmann K., Naumann V., Großer S. and Hagendorf C., 2015, “Methods for resistivity and thickness measurements of high resistivity interfacial layers in photovoltaic TCO multilayers”, Proc. 42nd IEEE PVSC.

Krause S., Kaufmann K., Lancaster K., Naumann V., Großer S., Hagendorf C., 2016, “Fs-laser micro machining for µ-TLM resistivity test structures in photovoltaic TCO multilayers”, SPIE Optics and Photonics.

Liu J. M., 1982, “Simple technique for measurements of pulsed Gaussian-beam spot sizes”, Optics Letters 7 , 196.

Olbrich, M., Punzel, E., Roesch, R. *et al.,* 2016, “Case study on the ultrafast laser ablation of thin aluminum films: dependence on laser parameters and film thickness”, *Appl. Phys. A* 122, 215.

Schroder D. K., 2015, “Semiconductor material and device characterization, John Wiley & Sons.